Vítor Monteiro, Tiago J. C. Sousa, M. J. Sepúlveda, Carlos Couto, António Lima, João L. Afonso

**"A Proposed Bidirectional Three Level dc dc Power Converter for Applications in Smart Grids: An Experimental Validation"**

IEEE SEST International Conference on Smart Energy Systems and Technologies, Porto, Portugal, Sept. 2019.

Vítor Monteiro, Tiago J. C. Sousa, M. J. Sepúlveda, Carlos Couto, António Lima, João L. Afonso, "A Proposed Bidirectional Three Level dc dc Power Converter for Applications in Smart Grids: An Experimental Validation", IEEE SEST International Conference on Smart Energy Systems and Technologies, Porto, Portugal, Sept. 2019.

# A Proposed Bidirectional Three-Level dc-dc Power Converter for Applications in Smart Grids: An Experimental Validation

Vítor Monteiro
Industrial Electronics Department
ALGORITMI Research Centre
University of Minho
Campus de Azurem, Portugal
vmonteiro@dei.uminho.pt

Tiago J. C. Sousa
Industrial Electronics Department
ALGORITMI Research Centre
University of Minho
Campus de Azurem, Portugal
tsousa@dei.uminho.pt

M. J. Sepulveda
Industrial Electronics Department
ALGORITMI Research Centre
University of Minho
Campus de Azurem, Portugal
mjs@dei.uminho.pt

Carlos Couto
Industrial Electronics Department
ALGORITMI Research Centre
University of Minho
Campus de Azurem, Portugal
ccouto@dei.uminho.pt

Antonio Lima
Electrical Engineering Department
University of the State of
Rio de Janeiro
Brazil
antoniolima@uerj.br

Joao L. Afonso
Industrial Electronics Department
ALGORITMI Research Centre
University of Minho
Campus de Azurem, Portugal
jla@dei.uminho.pt

***Abstract*—The integration of renewable energy sources (RES), energy storage systems (ESS), and electric mobility into smart grids requires the use of dc-dc back-end power converters for adjusting voltage levels. Although a dc-dc converter applied for RES only operates in unidirectional mode, when applied to ESS or EM, the bidirectional mode is a fundamental requisite for exchanging power with the electrical power grid. In this context, this paper presents an experimental validation of a proposed bidirectional three-level dc-dc converter considering its application for smart grids. Traditionally, the dc-dc power converters of such applications are two-level converters. However, by employing a three-level topology, it is possible to improve the quality of the variables controlled by the power converter. Moreover, since the proposed dc-dc converter is controlled to produce a controlled current, the proposed current control and modulation strategies are introduced and described. A complete analysis of the operation principle of the proposed bidirectional three-level dc-dc power converter is presented, supported by experimental validation, employing a laboratory prototype.**

***Keywords—dc-dc Converter; Electric Mobility; Energy Storage System; Renewable Energy Source; Smart Grids.***

## I. INTRODUCTION

Nowadays, the subject of sustainable electrical energy is recognized as one of the utmost societal challenges for future generations. In fact, smart grids are identified as a fundamental contribution for a sustainable electrical energy, proving a set of new valences concerning the adoption of renewable energy sources (RES), electric mobility, and energy storage systems (ESS) [1][2]. The introduction of these valences are also of paramount interest for providing improvements in terms of energy efficiency in all energy sectors, as well as in terms of power quality and optimization of the electrical loads based on the customer perspective. A complete and comprehensive study about these technologies, concerning the state-of-the-art and future vision, is offered in [3]. A flexible control of the charging requirements for electric mobility to meet the RES production as a contribution for minimizing GHG emissions is proposed in [4]. The combination of electric mobility maximizing the power production from RES is illustrated in [5] as an influence for the sustainability of the transportation and electrical energy sectors. The behavior of the electric mobility as a contribution for stabilizing the grid voltage, also considering RES, is presented in [6]. Similar studies can be found in [7], [8], [9], and [10]. Also framing all of these three strands prospecting an economic deployment, a hybrid strategy is proposed in [12]. An overview of technologies for electric mobility including energy storage systems and electrical motors is presented in [13].

Nevertheless, enhancing the introduction of these technologies in smart grids, aiming to accommodate the needs of all players, requires the use of power converters [14]. Characteristically, these technologies are interfaced with the power grid by means of different and individual equipment (constituted by a combination of an ac-dc with a dc-dc [15][16]. Analyzing from the power grid, each technology has an ac-to-dc converter and a dc-dc converter. With a view to contributing to increase efficiency, unified topologies with a single ac-side interface and multiple dc-side interfaces are emerging, both in terms of controllability and power structures. Therefore, different ac-dc topologies can be adopted [17][18]. An experimental validation of an integrated topology with a single ac-side interface, but with two dc-side interfaces, is presented in [19]. Similar topologies using three converters are investigated in [20] and [21], however, only considering the possibility of the electrical mobility in unidirectional mode. An arrangement for interfacing off-board chargers of electric mobility and RES with the grid is presented in [22], neglecting a discussion about the topology used and about the control algorithm. A multimode single-leg converter is offered in [23] for controlling the power flow between RES and ESS, but without the grid interface. A multi-port structure is considered in [24], however, requiring two converters in the ac-side. In this context, this paper presents a three-level bidirectional dc-dc converter that can be used in applications requiring three dc interfaces. As example, one of the interfaces is to connect a dc-to-ac converter for the grid interface, while the other two interfaces can connect, e.g., RES and ESS. However, since the converter can be used for various purposes in smart grids, it can also be used for RES interface and electric mobility (off-board systems), or ESS and electric mobility (off-board). Thus, the main advantages of the proposed converter consist of: (i) Operation with a

978-1-7281-1156-8/19/$31.00 ©2019 IEEE

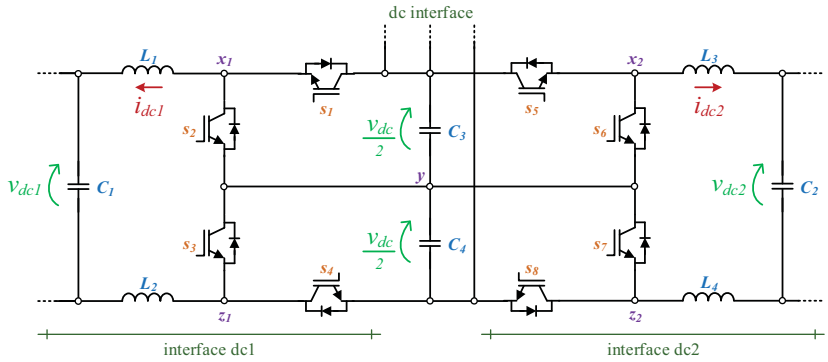


Fig. 1. Topology of the proposed bidirectional three-level dc-dc power converter for applications in smart grids.

control scheme similar to an interleaved converter, controlling the variables with the double of the switching frequency; (ii) Operation with three voltage levels; (iii) Possibility of exchanging power directly between dc systems in bidirectional mode; (iv) Low number of electronic components. The computational and experimental validation presented in the paper show that the converter operates as intended, proving that it has an added value for unified converters in smart grids.

TABLE I
POSSIBLE STATES OF THE PROPOSED DC-DC CONVERTER

| | $s1$ | $s2$ | $s3$ | $s4$ | $s5$ | $s6$ | $s7$ | $s8$ | $v_{x1y1}$ | $v_{y1z1}$ | $v_{x2y2}$ | $v_{y2z2}$ |
|---|---|---|---|---|---|---|---|---|---|---|---|---|
| #1 | 1 | 0 | 0 | 0 | 1 | 0 | 0 | 0 | $v_{dc}/2$ | 0 | $v_{dc}/2$ | 0 |
| | 0 | 0 | 0 | 1 | 0 | 0 | 0 | 1 | 0 | $v_{dc}/2$ | 0 | $v_{dc}/2$ |
| | 0 | 0 | 0 | 0 | 0 | 0 | 0 | 0 | 0 | 0 | 0 | 0 |
| | 1 | 0 | 0 | 1 | 1 | 0 | 0 | 1 | $v_{dc}/2$ | $v_{dc}/2$ | $v_{dc}/2$ | $v_{dc}/2$ |
| #2 | 0 | 1 | 0 | 0 | 0 | 1 | 0 | 0 | 0 | $v_{dc}/2$ | 0 | $v_{dc}/2$ |
| | 0 | 0 | 1 | 0 | 0 | 0 | 1 | 0 | $v_{dc}/2$ | 0 | $v_{dc}/2$ | 0 |
| | 0 | 1 | 1 | 0 | 0 | 1 | 1 | 0 | 0 | 0 | 0 | 0 |
| | 0 | 0 | 0 | 0 | 0 | 0 | 0 | 0 | $v_{dc}/2$ | $v_{dc}/2$ | $v_{dc}/2$ | $v_{dc}/2$ |
| #3 | 1 | 0 | 0 | 0 | 0 | 1 | 0 | 0 | $v_{dc}/2$ | 0 | 0 | $v_{dc}/2$ |
| | 0 | 0 | 0 | 1 | 0 | 0 | 1 | 0 | 0 | $v_{dc}/2$ | $v_{dc}/2$ | 0 |
| | 0 | 0 | 0 | 0 | 0 | 1 | 1 | 0 | 0 | 0 | 0 | 0 |
| | 1 | 0 | 0 | 1 | 0 | 0 | 0 | 0 | $v_{dc}/2$ | $v_{dc}/2$ | $v_{dc}/2$ | $v_{dc}/2$ |
| #4 | 0 | 1 | 0 | 0 | 1 | 0 | 0 | 0 | 0 | $v_{dc}/2$ | $v_{dc}/2$ | 0 |
| | 0 | 0 | 1 | 0 | 0 | 0 | 0 | 1 | $v_{dc}/2$ | 0 | 0 | $v_{dc}/2$ |
| | 0 | 1 | 1 | 0 | 0 | 0 | 0 | 0 | 0 | 0 | 0 | 0 |
| | 0 | 0 | 0 | 0 | 1 | 0 | 0 | 1 | $v_{dc}/2$ | $v_{dc}/2$ | $v_{dc}/2$ | $v_{dc}/2$ |

## II. PROPOSED DC-DC TOPOLOGY

The topology is shown in Fig. 1, where for other applications the same topology can be applied, such as: multilevel dc-dc converters [25]; ultracapacitors [26][27]; automotive applications [28][29]. In total, eight fully controlled power semiconductors are employed in order to operate in bidirectional mode. It is important to note that the topology can operate with only one of the dc interfaces, since it can be seen as two dc-dc converters. In addition, the eight semiconductors are never controlled at the same time, i.e., if only one dc interface is required, two semiconductors are controlled, and if two dc interfaces are required, four semiconductors are controlled. This aspect is of particular interest and it is always valid regardless of the power flow (e.g., whether the ESS is charging or discharging). Table I summarizes the various states that the converter can take depending on each operation mode. The table is divided into four cases of operation. Case #1 corresponds to a situation in which both dc interfaces are receiving power from the dc-link. Quite the opposite, case #2 corresponds to a situation in which both interfaces are providing power to the dc-link. Case #3 corresponds to the mode in which the dc1 interface is receiving power and the dc2 interface is supplying power. In this case, the dc1 interface may receive power from the dc-link or from the dc2 interface, or from both sides. Finally, case #4 is the analogue case of case #3, where the dc1 interface is supplying power and the dc2 interface is receiving power. Also in this case it is important to note that the dc2 interface may receive power from the dc-link or from the dc1 interface, or from both sides.

## III. DIGITAL CONTROL IMPLEMENTATION

This section evaluates the feedback control and the pulse-width modulation (PWM) used for controlling the converter according to the different cases enumerated in Table I. Based on such cases, by applying an appropriate control strategy in terms of PWM, the converter can operate in a similar manner to a conventional interleaved converter. Considering one of the dc interfaces as example, the current in both inductors ($L_1$ and $L_2$) is almost the same, but the ripple frequency of the current is twice the switching frequency of each semiconductor. This principle applies to any of the cases identified in Table I, permitting to reduce the requirements of the coupling filters. Each dc interface can be individually controlled, allowing either current or voltage feedback control (according to the necessities of the dc interface, typically performed with current feedback control), which is implemented using a fixed frequency predictive control technique. For simplicity, only one of the dc interfaces is analyzed. It is important to note that, since two carriers are used (shifted 180 degrees), it makes sense to use both carriers for controlling two variables (as in equations (1) and (2)). The two carriers and two control variables are fundamental for the operation similar to an interleaved operation. So, when the interface is receiving power, it can be established that:

$$v_{x1y} = v_{L1} + v_{L2} + v_{dc1}\,, \tag{1}$$

$$v_{yz1} = v_{L1} + v_{L2} + v_{dc1}\,, \tag{2}$$

where $v_{x1y}$ and $v_{yz1}$ represent the voltages that the converter can assume, $v_{L1}$ and $v_{L2}$ are the voltages in the inductors $L_1$ and $L_2$, and $v_{dc1}$ is the voltage at the interface dc1. Considering that the current in the inductor $L_1$ is the same as in the inductor $L_2$, replacing the voltages in the inductor yields:

$$v_{x1y} = (L_1 + L_2)\frac{di_{L1}}{dt} + v_{dc1}\,, \tag{3}$$

$$v_{yz1} = (L_1 + L_2)\frac{di_{L2}}{dt} + v_{dc1}\,. \tag{4}$$

Using the forward Euler method for discretizing the equations, the digital implementation can be done as:

$$v_{x1y}[k] = \frac{L_1 + L_2}{T_s}(i_{L1}[k+1] - i_{L1}[k]) + v_{dc1}\,, \quad (5)$$

$$v_{yz1}[k] = \frac{L_1 + L_2}{T_s}(i_{L1}[k+1] - i_{L1}[k]) + v_{dc1}\,, \quad (6)$$

where $i_{L1}[k+1]$ and $i_{L2}[k+1]$ are the currents to be reached at time $[k+1]$. Knowing that the frequency of the ripple in the current is intended to be twice the switching frequency, two triangular carriers, shifted 180 degrees in relation to the other, are used. The control signals for the semiconductors *s1* and *s4* are obtained by comparing the voltages that the converter must produce ($v_{x1y}$ and $v_{yz1}$) with the two triangular carriers. When the dc interface is providing power (the equations are different, since the converter, in this case, will operate in boost mode instead of the aforementioned mode in buck mode), analyzing Fig. 1, it can be established that:

$$v_{x1y} = v_{dc1} - v_{L1} - v_{L2}\,, \quad (7)$$

$$v_{yz1} = v_{dc1} - v_{L1} - v_{L2}\,, \quad (8)$$

Replacing the voltages in the inductors $L_1$ and $L_2$ yields:

$$v_{x1y} = v_{dc1} - (L_1 + L_2)\frac{di_{L1}}{dt}\,, \quad (9)$$

$$v_{yz1} = v_{dc1} - (L_1 + L_2)\frac{di_{L1}}{dt}\,, \quad (10)$$

Again, using the aforementioned Euler method, the digital implementation of the equations can be done as:

$$v_{x1y}[k] = v_{dc1} - \frac{L_1 + L_2}{T_s}(i_{L1}[k+1] - i_{L1}[k])\,, \quad (11)$$

$$v_{yz1}[k] = v_{dc1} - \frac{L_1 + L_2}{T_s}(i_{L1}[k+1] - i_{L1}[k])\,, \quad (12)$$

where $i_{L1}[k+1]$ is the current to be reached at time $[k+1]$. Also in this mode of operation (where the dc interface provides power), two triangular carriers, shifted 180 degrees in relation to the other, are used. The control signals for the semiconductors *s2* and *s3* are obtained by comparing the voltages that the converter must produce ($v_{x1y}$ and $v_{yz1}$) with the two triangular carriers. Next, several results for operation in steady-state and transient-state are presented, as well as for operation in bidirectional mode, always ensuring a proper current control based on the established reference. Thus, for the dc-link, it was considered a voltage of 800 V, divided into 400 V for each part (split dc-link with symmetrical voltages). For validating the principle of operation and the proposed control, only one of the dc interfaces was considered, since both are governed by the same operating logic. As it will be seen in the results, initially, for the interface dc1, a voltage of 100 V was considered (less than 400 V, i.e., less than half of the dc-link voltage) and, subsequently, a voltage of 500 V was considered, which corresponds to a value higher than 400 V (more than half of the dc-link voltage). As a passive filter, an inductance of 1 mH was considered. The switching frequency of each semiconductor was set at 20 kHz, which corresponds to half the sampling frequency (40 kHz) of the control algorithm. The control was implemented in *C* language, using all the equations previously presented.

In Fig. 2 is presented a result that shows the main variables used in the control algorithm, considering the operation in steady-state, thus validating the operation of the proposed converter when the interface dc1 is receiving energy. In particular, this result allows to validate the current control, since it is verified that the current $i_{dc1}$ follows its reference $i_{dc1}$* and whose ripple frequency corresponds to twice the switching frequency (it is emphasized that this characteristic of operating in a mode similar to an interleaved converter is one of the most relevant features of the proposed converter). This result also validates the voltage assumed by the converter, in which case it assumes values 0 and $v_{dc}/2$, since the dc interface voltage is less than half the dc-link voltage. The control signals of each semiconductor (*s1* and *s4*) are obtained by comparing, respectively, the reference voltages $v_{pwm\_s1}$ and $v_{pwm\_s4}$ with the triangular carriers $tri_a$ and $tri_b$ (as shown, with a phase shift of 180 degrees from each other). Since the difference between the dc interface voltage ($v_{dc1}$) is four times less than half of the dc-link voltage ($v_{dc}/2$) and as the converter operates with an interleaved control structure, the duty-cycle value of the control signal of each semiconductor is about 12.5%.

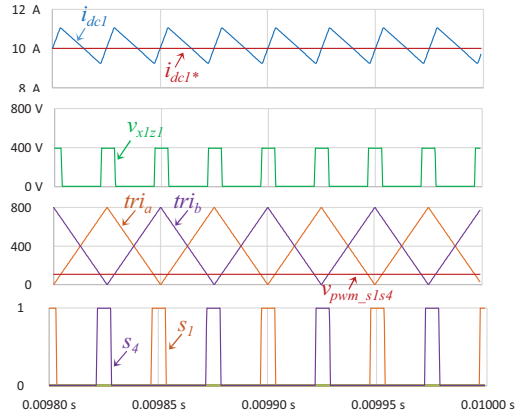


Fig. 2. Simulation results in steady-state when the interface dc1 is receiving power from the dc-link.

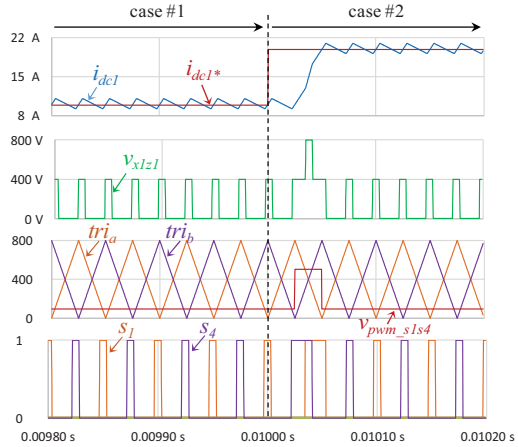


Fig. 3. Simulation results in transient-state when the interface dc1 is receiving power from the dc-link, and considering a sudden variation of the reference of current.

In Fig. 3 the same variables are presented as in the previous case, but considering the operation in transient-state, where the current reference changes to the double in a sudden transition. As it turns out, again in this case, the current ($i_{dc1}$) follows its reference ($i_{dc1}$*) even with the abrupt change that has occurred. However, this result was mainly obtained to verify the voltage levels that the converter takes on transient-state. Thus, in the transition, for the current to follow the reference in the shortest possible time, the

converter assumes the three permitted voltage levels, i.e., 0, $v_{dc}/2$ and $v_{dc}$. In this case, since the reference voltage values ($v_{pwm\_s1}$ and $v_{pwm\_s4}$) are greater than half the maximum amplitude of the triangular carrier, the control signals of the semiconductors (*s1* and *s4*) are both active at the same time (i.e., they are overlapped, meaning that the voltage of the converter $v_{x1z1}$ assumes the value $v_{dc}$, forcing the current to reach its reference). In this specific case, temporarily, the duty-cycle increased about four times in relation to the steady-state. Fig. 4 shows a similar result to the previous one, but considering the transient-state when the current reference is halved and when the interface dc1 is providing power. In this case, since the interface dc1 is providing power to the dc-link, the current is represented with a negative value, which is only due to the position of the current sensor (this is because the sensor is fixed in a certain position regardless the operation mode). Also in this case, it is verified that the current ($i_{dc1}$) follows its reference ($i_{dc1}$*), but as it is a decrease of the reference current, the converter only assumes the values of 0 and $v_{dc}/2$. In this case, only the semiconductors *s2* and *s3* are used, with the control signals of each semiconductor (*s2* and *s3*) being obtained by comparing, respectively, the reference voltages $v_{pwm\_s2}$ and $v_{pwm\_s3}$ with the triangular carriers $tri_a$ and $tri_b$. As in the previous cases, it is found that the current ripple frequency is twice the switching frequency. In this specific case, transiently, the duty-cycle of each semiconductor increases about to the double. By combining the previous cases in a single case, Fig. 5 shows the transition from the case when the interface dc1 is providing power, to the mode in which the same interface receives power. This mode has been considered for validation and can be interpreted as an extreme operating condition of the converter, where the current reference ($i_{dc1}$*) changes instantly from a negative value to a positive value. For example, in a practical situation, this mode may correspond to the use of ESS as dc interface, in which it is discharging and then is charging. As it turns out, for this change to take place in the shortest possible time, the converter voltage, transiently, assumes the three possible values, 0, $v_{dc}/2$ and $v_{dc}$. Initially, only the semiconductors *s2* and *s3* are controlled (when the interface dc1 is providing power), and then only the semiconductors *s1* and *s4* are controlled (when the interface dc1 is receiving power). Fig. 6 presents a result, also in transient-state, when the interface dc1 is receiving power, but differently from the previous cases, instead of changing the current reference, a change in the interface dc1 voltage was considered. Thus, initially a voltage of 100 V (which is a voltage value less than $v_{dc}/2$) was used, and subsequently, for about 1.6 ms, that voltage was gradually increased to 500 V (which is a value higher than $v_{dc}/2$). With this result, it is verified that the current ($i_{dc1}$) always follows its reference ($i_{dc1}$*), but the voltage assumed by the converter changes according to the voltage value of the interface dc1. When the interface dc1 voltage is less than $v_{dc}/2$, the converter voltage varies between 0 and $v_{dc}/2$, but when the interface dc1 voltage is greater than $v_{dc}/2$, the converter voltage varies between $v_{dc}/2$ and $v_{dc}$, verifying the operation of the proposed converter with three different levels of operation. As it turns out, the voltage level transition only occurs when the interface dc1 voltage is equal to half the dc-link voltage. More importantly, when both voltages assume equal values, the current ripple assumes the lowest possible value. Thus, it is easy to conclude that the closer the voltage values of the interface dc1 and the dc-link, the smaller the current ripple.

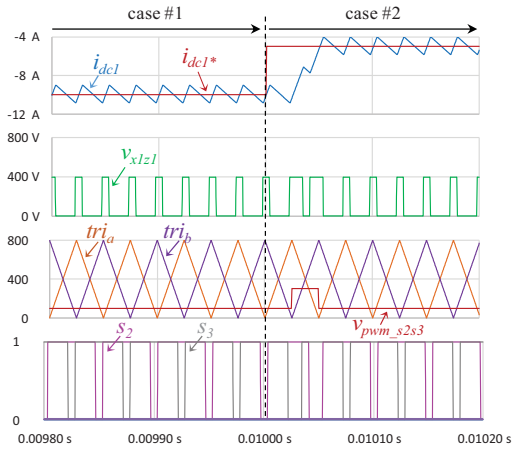


Fig. 4. Simulation results in transient-state when the interface dc1 is providing power to the dc-link, and considering a sudden variation of the reference of current.

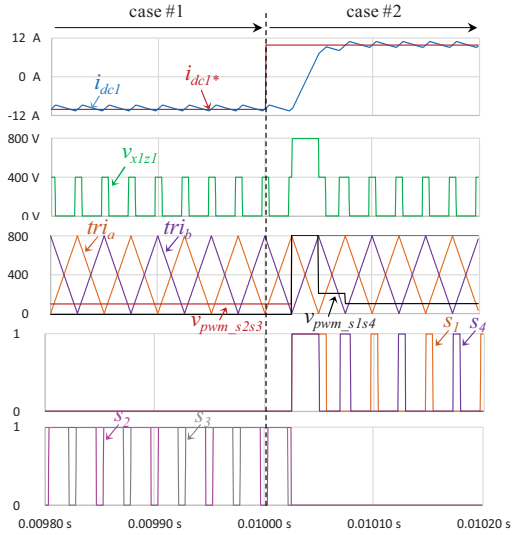


Fig. 5. Simulation results in transient-state considering a sudden variation in the reference of current: Case #1 when the interface dc1 is providing power to the dc-link; Case #2 when the interface dc1 is receiving power from the dc-link.

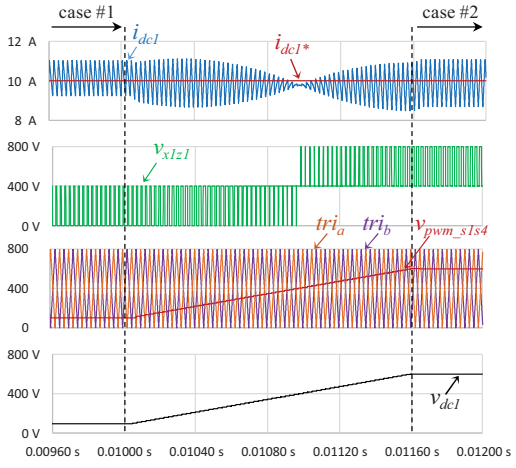


Fig. 6. Simulation results in transient-state when the interface dc1 is receiving power from the dc-link, and considering a smooth variation of the voltage in the interface dc1.

## IV. Prototype Implementation and Experimental Verification

In Fig. 7 is presented the developed prototype (IGBT Semikron SKM100GB125DN, gate drivers SKHI21A(R),

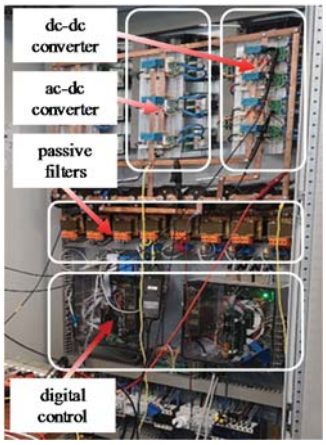


Fig. 7. Developed prototype composed by the proposed dc-dc power converter and by a dc-ac power converter to interface with the power grid.

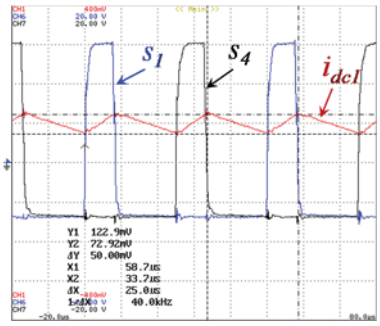


Fig. 8. Experimental results of the proposed dc-dc converter when the interface dc1 is receiving power from the dc-link.

F28335 DSP, LEM sensors. The sampling frequency was set at 40 kHz and the switching frequency at 20 kHz. The used filters were: $L_1$=$L_2$=$L_3$=$L_4$=1 mH, and $C_1$=$C_2$=1 mF. It is important to note that a dc-source and a resistor were used for emulating the battery (during the discharging and discharging, respectively) and a dc-source with a series resistor was used to emulate a set of PV panels. These systems were used, since the main goal was to validate the topology and the control algorithms. A voltage of 150 V was used in the dc-link. In Fig. 8 is presented an experimental result that shows in detail the gate-emitter voltage in the IGBTs *s1* and *s4*, as well as the obtained current ($i_{dc1}$). In this result, it is verified that the current is positive, meaning, according to the position of the sensor, that the interface dc1 is receiving power. In this result, it is also visible that the resulting frequency corresponds to twice the switching frequency. It is important to note that the current was measured, specifically, in order to show the ripple value and the ripple frequency value (40 kHz). In Fig. 9 is presented a result that corresponds to the case where the interface dc1 is providing power. For this reason, the current assumes negative values. This result shows in detail the gate-emitter voltage in the IGBTs *s2* and *s3*, as well as the current obtained ($i_{dc1}$).

Fig. 10 shows a complete result in which both interfaces are operating and interconnected with the ac-to-dc interface. Initially, in case #1, the interface dc1 is supplying power and, in case #2, in addition to the interface dc1, the interface dc2 receives power. As a practical example, a RES interface (interface dc1) and a battery interface (dc2) were considered for this result. In order to obtain a result with distinct operation of both interfaces, it was considered the charging process of the batteries. Thus, the interface dc1 provides

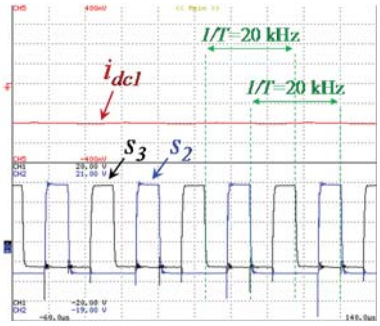


Fig. 9. Experimental results of the proposed dc-dc power converter when the interface dc1 is providing power to the dc-link.

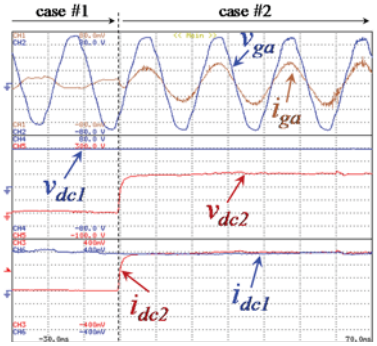


Fig. 10. Experimental results of the proposed dc-dc power converter and dc-ac power converter: Case #1 when the interface dc1 is providing power to the dc-link, which is injected into the power grid through the dc-ac converter, and the interface dc2 is inactive; Case #2 when the interface dc1 is providing power to the dc-link and the interface dc2 is receiving power from the dc-link (since the power from the interface dc1 is greater than the power necessary for the interface dc2, a parcel of power is absorbed from the ac power grid through the dc-ac converter).

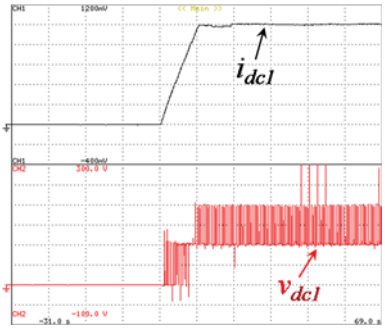


Fig. 11. Experimental results of the interface dc1 concerning the current and the three voltage levels.

power (as RES, the interface is unidirectional and hence the current value is always positive, i.e., the current sensor measures as positive from the RES) and the interface dc2 receives power (i.e., the current sensor measures as positive from the dc-link and as negative to the dc-link).

As it can be seen, due to the operation of the dc-dc converter, on the power grid side, in case #1 the current is in phase opposition to the voltage (power from RES is injected into the grid) and, in case #2, the current is in phase with the voltage (the operating power of the interface dc2 is higher than the interface dc1, therefore, a parcel of power is absorbed from the grid to the interface dc2). Fig. 11 shows the current on the interface dc1, as well as the three voltage levels also in this interface. Concerning the efficiency, it is important to note that the switching losses is an important aspect, however, since the prototype can work in different operation modes (e.g., with different power levels from renewables) the calculation of the switching and conduction

losses is very extensive (for contemplating all the possibilities). Therefore, such analysis is under study for a future improved paper also related with this topic.

## V. Conclusions

In a context of smart grids, where the use of unified converters is an added-value to the integration of renewable energy sources (RES), energy storage systems (ESS) and electric mobility, the use of dc-dc bidirectional converters with multiple dc interfaces will be of great importance. Thus, this paper presented a dc-dc power converter with three bidirectional interfaces (one of them for interfacing a dc-ac power converter connected to the power grid). In addition to allowing the operation in bidirectional mode, it also allows to exchange power directly between dc interfaces, and according to the voltage value of the dc interfaces, the power converter operates with three voltage levels. As analyzed and verified, another of the advantages of the proposed converter is that it allows to operate with a control that forces its output variable to be controlled with a frequency that is twice the switching frequency, i.e., similarly to an interleaved converter. A complete analysis of the operation principle of the proposed converter, based on several operation modes, is presented in detail and supported by an experimental validation using a developed laboratory prototype.

## Acknowledgment

This work has been supported by FCT – Fundação para a Ciência e Tecnologia within the Project Scope: UID/CEC/00319/2019. This work has been supported by FCT Project *DAIPESEV* PTDC/EEI-EEE/30382/2017, and by the FCT Project *newERA4GRIDs* PTDC/EEI-EEE/30283/2017. Tiago Sousa is supported by the doctoral scholarship SFRH/BD/134353/2017 granted by FCT.

## References

[1] Wencong Su, Habiballah Rahimi-Eichi, Wente Zeng, Mo-Yuen Chow, "A Survey on the Electrification of Transportation in a Smart Grid Environment," IEEE Trans. Ind. Informat., vol.8, no.1, pp.1-10, Feb. 2012.

[2] Sagar K. Rastogi, Arun Sankar, Kushagra Manglik, Santanu K. Mishra, Saraju P. Mohanty, "Toward the Vision of All-Electric Vehicles in a Decade," IEEE Consumer Electronics Magazine, pp.103-107, Mar. 2019.

[3] Alireza Khaligh, Zhihao Li, "Battery, Ultracapacitor, Fuel Cell, and Hybrid Energy Storage Systems for Electric, Hybrid Electric, Fuel Cell, and Plug-In Hybrid Electric Vehicles: State of the Art," IEEE Trans. Veh. Technol., vol.59, no.6, pp.2806-2814, July 2010.

[4] Jorge E. Hernandez, Frank Kreikebaum, Deepak Divan, "Flexible Electric Vehicle (EV) Charging to Meet Renewable Portfolio Standard (RPS) Mandates and Minimize Green House Gas Emissions," IEEE ECCE Energy Conversion Congress and Exposition, Atlanta USA, pp.4270-4277, Sept. 2010.

[5] Ahmed Yousuf Saber, Ganesh Kumar Venayagamoorthy, "Plug-in Vehicles and Renewable Energy Sources for Cost and Emission Reductions,"IEEE Trans. Ind. Electron., vol.58, no.4, pp.1229-1238, Apr. 2011.

[6] Willett Kempton, Jasna Tomic, "Vehicle-to-Grid Power Implementation: From Stabilizing the Grid to Supporting Large-Scale Renewable Energy," ELSEVIER Journal of Power Sources, vol.144, pp.280-294, Apr. 2015.

[7] Jun Hua Zhao, Fushuan Wen, Zhao Yang Dong, Yusheng Xue, Kit Po Wong, "Optimal Dispatch of Electric Vehicles and Wind Power Using Enhanced Particle Swarm Optimization," IEEE Trans. Ind. Informat., vol.8, no.4, pp.889-899, Nov. 2012.

[8] Iban Junquera Martinez, Javier Garcia-Villalobos, Inmaculada Zamora, Pablo Eguia, "Energy Management of Micro Renewable Energy Source and Electric Vehicles at Home Level ," SPRINGER Journal of Modern Power Systems and Clean Energy, vol.5, no.6, pp.979-990, Nov. 2017.

[9] Wayes Tushar, Chau Yuen, Shisheng Huang, David B. Smith, H. Vincent Poor, "Cost Minimization of Charging Stations With Photovoltaics: An Approach with EV Classification," IEEE Trans. Intell. Transp. Syst., vol.17, no.1, pp.156-169, Jan. 2016.

[10] Shuang Gao, K. T. Chau, Chunhua Liu, Diyun Wu, C. C. Chan, "Integrated Energy Management of Plug-in Electric Vehicles in Power Grid With Renewables," IEEE Trans. Veh. Technol., vol.63, no.7, pp.3019-3027, Sept. 2014.

[11] Mosaddek Hossain Kamal Tushar, AdelW. Zeineddine, Chadi Assi, "Demand-Side Management by Regulating Charging and Discharging of the EV, ESS, and Utilizing Renewable Energy," IEEE Trans. Ind. Informat., vol.14, no.1, pp.117-126, Jan. 2018.

[12] Kalpesh Chaudhari, Abhisek Ukil, K Nandha Kumar, Ujjal Manandhar, Sathish Kumar Kollimalla, "Hybrid Optimization for Economic Deployment of ESS in PV-Integrated EV Charging Stations," IEEE Trans. Ind. Informat., vol.14, no.1, pp.106-116, Jan. 2018.

[13] Ali M. Bazzi, Yiqi Liu, Daniel S. Fay, "Electric Machines and Energy Storage: Over a century of technologies in electric and hybrid electric vehicles," IEEE Electrification Magazine, pp.49-53, Sept. 2018.

[14] Vítor Monteiro, João C. Ferreira, Andrés A. Nogueiras Meléndez, João L. Afonso, "Model Predictive Control Applied to an Improved Five-Level Bidirectional Converter," IEEE Trans. Ind. Electron., vol.63, no.9, pp.5879-5890, Sept. 2016.

[15] Vitor Monteiro, João C. Ferreira, Andres A. Nogueiras Melendez, Carlos Couto, João L. Afonso, "Experimental Validation of a Novel Architecture Based on a Dual-Stage Converter for Off-Board Fast Battery Chargers of Electric Vehicles," IEEE Trans. Veh. Tech., vol.67, no.2, pp.1000-1011, Feb. 2018.

[16] Rafael Leite, João L. Afonso, Vítor Monteiro, "A Novel Multilevel Bidirectional Topology for On-Board EV Battery Chargers in Smart Grids," MDPI Energies, vol.11, no.12, pp.1-21, Dec. 2018.

[17] Vítor Monteiro, Andrés A. Nogueiras Meléndez, João L. Afonso, "Novel Single-Phase Five-Level VIENNA-Type Rectifier with Model Predictive Current Control," IEEE IECON Industrial Electronics Conference, pp.6413-6418, Nov. 2017.

[18] Vítor Monteiro, Andrés A. Nogueiras Meléndez, Carlos Couto, João L. Afonso, "Model Predictive Current Control of a Proposed Single-Switch Three-Level Active Rectifier Applied to EV Battery Chargers," IEEE IECON Industrial Electronics Conference, Florence Italy, pp.1365-1370, Oct. 2016.

[19] Vítor Monteiro, J. G. Pinto, João L. Afonso, "Experimental Validation of a Three-Port Integrated Topology to Interface Electric Vehicles and Renewables with the Electrical Grid", IEEE Trans. Ind. Informat., vol.14, no.6, pp 2364-2374, June 2018.

[20] Gustavo Gamboa, Christopher Hamilton, Ross Kerley, Sean Elmes, Andres Arias, John Shen, Issa Batarseh, "Control Strategy of a Multi-Port, Grid Connected, Direct-DC PV Charging Station for Plug-in Electric Vehicles," IEEE Energy Conversion Congress and Exposition, pp.1173-1177, Sept. 2010.

[21] Christopher Hamilton, Gustavo Gamboa, John Elmes, Ross Kerley, Andres Arias, Michael Pepper, John Shen, Issa Batarseh, "System Architecture of a Modular Direct-DC PV Charging Station for Plug-in Electric Vehicles," IEEE IECON Annual Conference on Industrial Electronics Society, pp.2516-2520, Nov. 2010.

[22] Joshua Traube, Fenglog Lu, Dragan Maksimovic, "Photovoltaic Power System with Integrated Electric Vehicle DC Charger and Enhanced Grid Support," EPE/PEMC International Power Electronics and Motion Control Conference, pp.1-5, Sept. 2012.

[23] Taesik Park, Taehyung Kim, "Novel Energy Conversion System Based on a Multimode Single-Leg Power Converter," IEEE Trans. Power Electron., vol.28, no.1, pp.213-220, Jan. 2013.

[24] Gustavo Gamboa, Christopher Hamilton, Ross Kerley, Sean Elmes, Andres Arias, John Shen, Issa Batarseh, "Control Strategy of a Multi-Port, Grid Connected, Direct-DC PV Charging Station for Plug-in Electric Vehicles," IEEE Energy Conversion Congress and Exposition, pp.1173-1177, Sept. 2010.

[25] M. Shen, F. Z. Peng, L. Tolbert, "Multilevel DC-DC Power Conversion System With Multiple DC Sources," IEEE Trans. Power Electron., vol.23, no.1, pp.420–426, Jan. 2008.

[26] P. Grbović, P. Delarue, P. Le Moigne, P. Bartholomeus, "A Bidirectional Three-Level DC-DC Converter for the Ultracapacitor Applications," IEEE Trans. Ind. Electron., vol.57, no.10, pp.3415–3430, Oct. 2010.

[27] P. Grbović, P. Delarue, P. Le Moigne, P. Bartholomeus, "The Ultracapacitor-Based Controlled Electric Drives With Braking and Ride-Through Capability: Overview and Analysis," IEEE Trans. Ind. Electron., vol.58, no.3, pp.925–936, Mar. 2011.

[28] Y. Du, X. Zhou, S. Bai, S. Lukic, A. Huang, "Review of non-isolated bi-directional DC-DC converters for plug-in hybrid electric vehicle charge station application at municipal parking decks," IEEE APEC Applied Power Electronics Conference and Exposition, pp.1145–1151. Feb. 2010.

[29] S. Dusmez, A. Hasanzadeh, A. Khaligh, "Comparative Analysis of Bidirectional Three-Level DC-DC Converter for Automotive Applications," IEEE Trans. Ind. Electron., vol.62, no.5, pp.3305–3315, May. 2015.